

# Bremsstrahlung in $\alpha$ Decay Reexamined

H. Boie,<sup>1</sup> H. Scheit,<sup>1</sup> U. D. Jentschura,<sup>1</sup> F. Köck,<sup>1</sup> M. Lauer,<sup>1</sup>

A. I. Milstein,<sup>2</sup> I. S. Terekhov,<sup>2</sup> and D. Schwalm<sup>1,\*</sup>

<sup>1</sup>*Max-Planck-Institut für Kernphysik, D-69117 Heidelberg, Germany*

<sup>2</sup>*Budker Institute of Nuclear Physics, 630090 Novosibirsk, Russia*

## Abstract

A high-statistics measurement of bremsstrahlung emitted in the  $\alpha$  decay of  $^{210}\text{Po}$  has been performed, which allows to follow the photon spectra up to energies of  $\sim 500$  keV. The measured differential emission probability is in good agreement with our theoretical results obtained within the quasi classical approximation as well as with the exact quantum mechanical calculation. It is shown that due to the small effective electric dipole charge of the radiating system a significant interference between the electric dipole and quadrupole contributions occurs, which is altering substantially the angular correlation between the  $\alpha$  particle and the emitted photon.

PACS numbers: 23.60.+e, 27.80.+w, 41.60.-m

The  $\alpha$  decay of an atomic nucleus is *the* archetypal quantum mechanical process, and so is the bremsstrahlung accompanied  $\alpha$  decay. It is therefore somewhat surprising that only ten years ago the first fully quantum mechanical calculation of the latter process has been performed, using first-order perturbation theory and the dipole approximation for the photon field [1]. On the other hand, it is known that the  $\alpha$  decay of a heavy nucleus and the radiation that accompanies this decay can be treated in the quasi-classical approximation as well, the applicability of this approximation being provided by the large value of the Sommerfeld parameter  $\eta$  [2, 3], which amounts to e.g.  $\eta = 22$  for the  $\alpha$  decay of  $^{210}\text{Po}$ . In all theoretical approaches the matrix element of bremsstrahlung incorporates contributions of the classically allowed and classically forbidden (tunneling) region. The relative contribution of the tunneling region is not small in general and can be interpreted as bremsstrahlung at tunneling. However, such an interpretation can only have a restricted meaning as the wavelength of the photon is much larger than the width of the tunneling region and even larger than the main classical acceleration region; it is therefore not possible to identify experimentally the region where the photon was emitted. Nevertheless, the issue of tunneling during the emission process was widely discussed [1, 2, 3, 4, 5, 6, 7]. The authors used different theoretical approaches leading to partly conflicting conclusions as to the contribution of the tunneling process to the bremsstrahlung, but - more seriously - also with regard to the energy dependent emission probabilities.

While the theoretical interest in the bremsstrahlung accompanied  $\alpha$  decay was stirred up by an experiment published in 1994 [8], this and later experimental attempts [9, 10] to observe these rare decays produced conflicting results and did not reach the sensitivity to allow for a serious test of the various theoretical predictions concerning the emission probabilities for  $\gamma$  energies above  $E_\gamma \sim 200$  keV. In the present paper we report on the first high-statistics measurement of bremsstrahlung in the  $\alpha$  decay of  $^{210}\text{Po}$ , where we have been able to observe the photon spectra up to  $E_\gamma \sim 500$  keV. Taking into account the interference between the electric dipole and quadrupole amplitudes, which we derived within the framework of a refined quasi-classical approximation [11], we find good agreement of our measured  $\gamma$  emission probabilities with those calculated in our quasi-classical approach as well as with the quantum mechanical prediction of Ref. [1].

The main experimental challenge is the very low emission rate for bremsstrahlung photons. Even with a rather strong  $\alpha$  source of  $\sim 100$  kBq the emission rate is only of the order

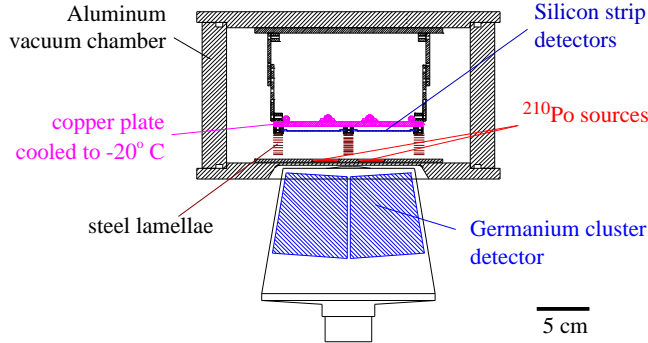


FIG. 1: (color online) Cross section of the experimental setup.

of *one per day* in the 300–400 keV energy range, i.e. in only one out of  $10^{10}$   $\alpha$  decays a photon with an energy within that range will be emitted. Only by measuring the  $\alpha$  particles in coincidence with the bremsstrahlung photons and by identifying the bremsstrahlung photons by requiring energy balance between the  $\alpha$  energy and the photon one can therefore hope to sufficiently suppress randoms due to the copious room background. After a careful evaluation of possible  $\alpha$  emitters,  $^{210}\text{Po}$ , already used in the work of Ref. [9], was felt to be the most promising choice for such a measurement. It decays with a half-life of  $t_{1/2} = 138$  days mainly to the ground state of the stable daughter nuclide  $^{206}\text{Pb}$  ( $Q_\alpha = 5.407$  MeV), with only a small fraction of  $1.22(4) \times 10^{-5}$  proceeding through the first excited  $J^\pi = 2^+$  state at an excitation energy of 803 keV [12]. While no other  $\gamma$  rays are emitted by the source, the weak 803 keV branch constitutes a convenient calibration point for the overall detection efficiency reached in the experiment.

The experimental setup used in the present work is shown in Fig. 1. Two  $^{210}\text{Po}$   $\alpha$  sources are placed at the bottom of a common vacuum chamber and are viewed by two segmented Silicon detectors, each placed about 30 mm above the source to measure the energy of the  $\alpha$  particles. Directly below the center of the vacuum chamber an efficient high-purity Germanium triple cluster detector of the MINIBALL design [13] was placed to record the emitted bremsstrahlung photons.

The source material was evenly spread on two 0.2 mm thick circular Ni foils with a diameter of 16 mm, which were mounted on Aluminum disks of 0.5 mm thickness each. By distributing the source material the  $\alpha$  energy loss in the material was minimized; moreover, sputtering of source material due to the recoil of a nearby  $\alpha$  decay was avoided. The areal uniformity of the activity (100 kBq per source) within the active area of the source was

tested by autoradiography; no intensity variations could be discerned.

The  $\alpha$  particles were detected by two  $5 \times 5 \text{ cm}^2$  Silicon detectors, which were electrically segmented into 16 strips each. The  $\alpha$  particles were incident on the unsegmented side of the detector in order to avoid events with incomplete charge collection occurring in the inter-strip region. Both detectors were mounted on a copper plate cooled to  $-20^\circ \text{ C}$  to improve the energy resolution and to reduce damage of the Si detectors due to the implanted  $\alpha$  particles (about  $10^{10} / \text{cm}^2$  at the end of experiment). The energy resolution was on the order of 30–35 keV (FWHM) and deteriorated only for a few strips up to 45 keV at the end of the production run. The direct path between the left source and the right Si detector (and vice versa) was mechanically blocked to avoid large angles of emission and incidence. Moreover, events with two responding strips were rejected in the off-line analysis, which considerably improved the low energy tail of the  $\alpha$  peaks. Typical counting rates were  $\sim 1.5 \text{ kHz}$  per strip.

The Ge cluster detector is comprised of three large volume and individually canned Ge crystals, which are housed in a common cryostat. Each crystal's outer electrode is electrically segmented into six wedge-shaped segments. The detector was equipped with fully digital electronics after the preamplifier, allowing to record not only the deposited energy but also the signal shapes of the 6 segments and the central core contact of a crystal with a sampling rate of 40 MHz. The segment hit pattern was used to determine the (first) interaction point of the photon, and the recorded pulse shapes were utilized to improve the  $\gamma$ - $\alpha$  time resolution (FWHM) to 29 ns at  $E_\gamma = 100 \text{ keV}$  and 15 ns at  $E_\gamma = 500 \text{ keV}$ . The  $\gamma$  energy was determined by adding the measured core energies of all three crystals. After carefully shielding the setup with copper and lead, the counting rate was as low as  $\sim 20 \text{ Hz}$  for a threshold at about 40 keV.

In view of the spreaded source and the close source-detector geometry, detailed simulations of the experimental setup were performed to determine the response function of the cluster detector as well as the detection efficiency of the setup as a function of  $E_\gamma$  and of the angle  $\vartheta$  between the direction of the  $\alpha$  particle and the bremsstrahlung quanta [14]. The simulated absolute  $\gamma$  full-energy peak efficiencies were compared to measurements performed with radioactive sources and to the result deduced from the 803 keV branch of the  $^{210}\text{Po}$  decay; their accuracies were found to be better than 4% for  $\gamma$  energies above 200 keV but to deteriorate slightly up to 9% at 100 keV. The absolute  $\gamma$  full-energy peak-efficiency at

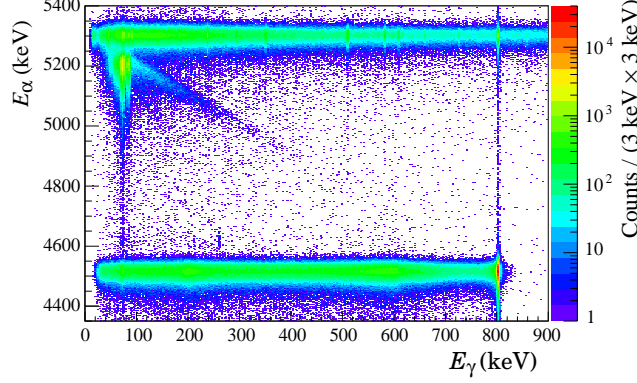


FIG. 2: (Color online) Scatter plot showing the energy of the  $\alpha$  particle versus the energy of the  $\gamma$  ray, detected coincident within a time window of  $\pm 50$  ns. The bremsstrahlung events can be clearly discerned along the diagonal line starting at  $E_\alpha = E_\alpha^0 = 5304$  keV.

803 keV was determined to be 8.09(26)% for isotropic emission.

In order to reach the necessary sensitivity the experiment had to be kept in a stable running condition for many months. The analyzed data actually correspond to 270 days of data taking with a total of  $4.3 \times 10^{11}$   $\alpha$  particles being recorded. At the same time about  $6 \times 10^9$   $\gamma$  rays have been detected out of which e.g. only about 150 are expected to be due to bremsstrahlung events in the  $\gamma$  energy region above 300 keV.

The  $\alpha$ - $\gamma$  coincidence matrix displaying the measured  $\alpha$  particle energy versus the  $\gamma$ -ray energy is shown in Fig. 2. The upper horizontal band corresponds to  $\alpha$  particles, which were detected with their full energy of  $E_\alpha^0 = 5304$  keV in random coincidence with a background photon. The lower horizontal band terminating at 803 keV  $\gamma$ -ray energy is caused by the response of the Ge detector to the 803 keV  $\gamma$ -rays, emitted in coincidence with  $\alpha$  particles of 4517 keV leading to the first excited state of  $^{206}\text{Pb}$ . The events at  $\gamma$  energies around between 70 keV and 85 keV for  $\alpha$  energies below 5304 keV correspond predominantly to Pb X-rays emitted after the knockout of an electron by the escaping  $\alpha$  particle [15]. Finally, on the diagonal line with  $E_\alpha + (206/210)E_\gamma = \text{const}$  as required by energy and momentum conservation, bremsstrahlung events can be clearly observed up to  $\gamma$  energies in excess of 400 keV.

To determine the differential bremsstrahlung emission probabilities  $dP/dE_\gamma$  coincident  $\alpha$ - $\gamma$  events with  $\gamma$  energies within 20 keV up to 100 keV broad gates were projected along the diagonal line by plotting them as a function of  $E_p = E_\alpha + (206/210)E_\gamma$ . For each  $\gamma$  gate the coincidence time window  $\Delta t$  was individually adjusted to include all counts

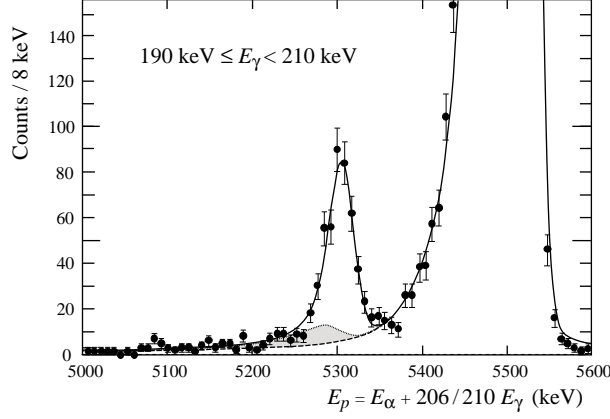


FIG. 3: Projected data and the result of a least-square fit (solid curve) for the  $\gamma$  energy bin of  $190 \text{ keV} \leq E_\gamma < 210 \text{ keV}$ . The peak centered at 5304 keV corresponds to the full-energy peak of photons from the bremsstrahlung accompanied  $\alpha$  decay, while the right structures is due to random  $\alpha$ - $\gamma$  coincidences.

within  $\pm 4.5 \sigma_t(E_\gamma)$  around the centroid of the time peak with  $\sigma_t^2$  denoting its variance. In the projected spectra the bremsstrahlung events are expected to show up in a sharp peak around  $E_p = E_\alpha^0 = 5304 \text{ keV}$  independent of the width of the  $\gamma$  energy gate. As an example, the projected energy spectrum for the  $190 \text{ keV} \leq E_\gamma < 210 \text{ keV}$  bin is shown in Fig. 3: Riding on the low energy tail of the random  $\alpha$ - $\gamma$  line the bremsstrahlung events are clearly born out. The solid curve corresponds to the result of a least-squares fit of the data, where only the intensity and central energy of the bremsstrahlung peak was varied. The line-shape and intensity of the random  $\alpha$ - $\gamma$  peak (dashed line) was determined from the corresponding projected energy spectrum of the random  $\alpha$ - $\gamma$  matrix, scaled by the ratio of the time windows. As the random matrix has  $\sim 10$  times more statistics, the tail under the bremstrahlung line could be determined to better than 5% for all  $\gamma$  energy gates. The shaded area reflects the Compton distribution caused by bremsstrahlung events with higher energies. Its intensity relative to the full energy events and its shape was determined from the simulation; the accuracy of this contribution is mainly determined by the intensities of the bremsstrahlungs peaks of the next higher  $\gamma$  gates and is estimated to be  $\sim 10\%$  for the bin shown in Fig. 3.

From the intensity of the bremsstrahlung line the (solid-angle integrated) differential emission probability  $dP(E_\gamma)/dE_\gamma$  can be determined if the total number of  $\alpha$  particles detected in the Si detectors,  $N_\alpha^0$ , and the probability to detect a bremsstrahlung photon of energy  $E_\gamma$  is known. While  $N_\alpha^0$  can be readily determined from the down-scaled single spectrum recorded

during the production run to be  $N_\alpha^0 = 4.311(2) \times 10^{11}$ , the detection efficiency requires some extra considerations as the photons are preferentially detected at backward angles with respect to the direction of the  $\alpha$  particle. Hence the  $\alpha$ - $\gamma$  angular correlation must be taken into account to extract the differential emission probability. Usually bremsstrahlung is assumed to be pure  $E1$  radiation as the wavelength of the emitted radiation is much larger than the dimension of the radiating system and higher order multipole contributions are suppressed. However, in the present case the radiating system consists of the  $\alpha$  particle *and* the residual daughter nucleus  $^{206}\text{Pb}$ , which have rather similar charge to mass ratios such that the effective dipole charge amounts only to  $Z_{E1}^{\text{eff}} = \mu(z/m - Z/M) = 0.40$ , where  $z, m$  and  $Z, M$  denote the charge and mass of the  $\alpha$  and the daughter nucleus, respectively, and  $\mu$  the reduced mass, while the effective quadrupole charge  $Z_{E2}^{\text{eff}} = \mu^2(z/m^2 + Z/M^2) = 1.95$  is almost a factor of 5 larger [11]. Even though one does not expect the  $E2$  radiation to contribute sizable to the total, angle integrated emission probability, the interference between the  $E1$  and  $E2$  amplitudes might well influence the  $\alpha$ - $\gamma$  angular correlation and thus the detection sensitivity of our setup.

We used a refined version of the quasi-classical approach to the bremsstrahlung emission process [11] to study this question in more detail, and find indeed a substantial  $E2/E1$  interference contribution to the angular correlation, while the  $E2$  contribution to the angle-integrated differential emission probability is less than 1.5% at all relevant  $\gamma$  energies. Including only the interference term the angular correlation can be expressed by  $dP(\vartheta)/d\Omega \propto \sin^2 \vartheta (1 + 2\chi(E_\gamma) \cos \vartheta)$ , where  $\chi(E_\gamma)$  is proportional to the ratio of the quadrupole to the dipole matrix element. In leading order in  $1/\eta$  we find that  $\chi(E_\gamma)$  approaches zero for  $E_\gamma \rightarrow 0$  and increases with  $E_\gamma$  to take e.g. values of +0.09 at 100 keV up to +0.22 at 500 keV. The influence of the  $E2$  amplitude on the angular correlation is illustrated in Fig. 4, where the normalized angular correlations of the emitted photons are shown as a function of  $\vartheta$  for bremsstrahlung photons of 100 keV and 500 keV in comparison to a pure dipole emission characteristic ( $\chi = 0$ ). Multiplied with the acceptance of our setup and integrated over the solid angle, the  $E2$  interference contribution results in a reduction of the detection efficiency of about 8% and 24% at photon energies of 100 and 500 keV, respectively, when compared to the efficiency expected for a pure dipole emission. From an estimate of the next to leading order contribution to  $\chi$  we can estimate the uncertainty to the detection efficiency caused by using only the leading order term in the angular correlation

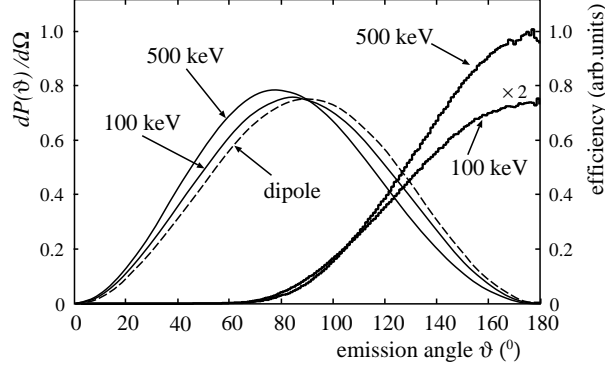


FIG. 4: Calculated, normalized  $\alpha$ - $\gamma$  correlations  $dP/d\Omega$  for bremsstrahlung photons of 100 and 500 keV in comparison to a pure dipole correlation. The increasing deviation from the dipole characteristic is due to the  $E2$  interference. Also shown are the emission angle dependent efficiencies (histograms) of our setup for photon energies of 100 keV and 500 keV.

to be less than 3%.

The resulting solid-angle integrated and efficiency corrected differential emission probabilities  $dP(E_\gamma)/dE_\gamma$  are displayed in Fig. 5 by the solid points. The  $1\sigma$  errors shown comprise the statistical and systematic uncertainties and are smaller than the point size for  $\gamma$  energies below 250 keV; they amount to e.g.  $\sigma_{sta} = 2\%$  and  $\sigma_{sys} = 8\%$  at  $\langle E_\gamma \rangle = 139$  keV, and  $\sigma_{sta} = 19\%$  and  $\sigma_{sys} = 5\%$  at  $\langle E_\gamma \rangle = 373$  keV. Also shown are the earlier results obtained by Kasagi *et al.* [9]. Note, that external bremsstrahlung contributions, which stem from the slowing down of the  $\alpha$  particles in the Si detector material, are several orders of magnitude smaller than the measured probabilities.

In Fig. 5 our data are also compared with the predictions of Papenbrock and Bertsch [1] and of our quasi-classical approach [11]; the two theoretical approaches actually agree with each other to better than 2% as shown in [11] and are thus indistinguishable on the scale of Fig. 5. Overall, very good agreement between theory and experiment is observed, however, small deviations of up to 20% are encountered at energies below 200 keV, which are also supported by the data of Kasagi *et al.* [9]. It remains to be seen if these deviations can be traced back to the use of the potential model so far employed in all theoretical calculations to describe the interaction of the  $\alpha$  particle and the daughter nucleus at distances of the order of the nuclear radius. The present high precision data clearly demonstrates the failure of a classical Coulomb acceleration calculation (see e.g. [9, 14]) to describe the bremsstrahlung



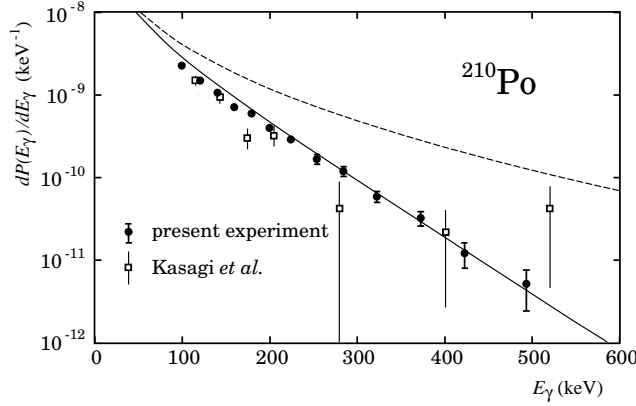


FIG. 5: Differential Bremsstrahlung emission probability  $dP(E_\gamma)/dE_\gamma$  for the decay of  $^{210}\text{Po}$  (solid points: present work, open symbols: Kasagi *et al.* [9]). The solid curve reflects the calculation of Papenbrock and Bertsch [1] as well as the result of our quasi-classical calculation [11]. The result of a classical Coulomb acceleration calculation is shown by the dashed line.

emission in  $\alpha$  decay, and rules out theoretical suggestions put forward by the authors of Refs. [6, 7, 9].

U.D.J. acknowledges support from the Deutsche Forschungsgemeinschaft (Heisenberg program) and D.S. support by a Joseph Meyerhoff Visiting Professorship granted by the Weizmann Institute of Science. A.I.M. and I.S.T. gratefully acknowledge the Max-Planck-Institute for Nuclear Physics, Heidelberg, for warm hospitality and support. The work was also supported by RFBR Grant No. 03-02-16510.

---

\* Present affiliation: Department of Particle Physics, Weizmann Institute of Science, Rehovot, Israel

- [1] T. Papenbrock and G. F. Bertsch, Phys. Rev. Lett. **80**, 4141 (1998).
- [2] M. I. Dyakonov and I. V. Gornyi, Phys. Rev. Lett. **76**, 3542 (1996).
- [3] M. I. Dyakonov, Phys. Rev. C **60**, 037602 (1999).
- [4] N. Takigawa *et al.*, Phys. Rev. C **59**, R593 (1999).
- [5] E. V. Tkalya, Phys. Rev. C **60**, 054612 (1999).
- [6] C. A. Bertulani, D. T. de Paula, and V. G. Zelevinsky, Phys. Rev. C **60**, 031602(R) (1999).
- [7] S. P. Maydanyuk and V. S. Olkhovsky, Prog. Theor. Phys. **109**, 203 (2003), and Eur. Phys. J. A **28**, 283 (2006).

- [8] A. D'Arrigo *et al.*, Phys. Lett. B **332**, 25 (1994).
- [9] J. Kasagi *et al.*, Phys. Rev. Lett. **79**, 371 (1997), Phys. Rev. Lett. **85**, 3062 (2000).
- [10] N. V. Eremin, G. Fazio, and G. Giardina, Phys. Rev. Lett. **85**, 3061 (2000).
- [11] U.D. Jentschura *et al.*, arXiv:nucl-th/0606005.
- [12] R.B. Firestone, *Table of Isotopes* (J. Wiley&Sons, New York,1996).
- [13] J. Eberth *et al.*, Prog. Part. Nucl. Phys. **46**, 389 (2001).
- [14] H. Boie, Dissertation, Univ. Heidelberg (2007).
- [15] H.J. Fischbeck, M.S. Freedman, Phys. Rev. Lett. **34**, 173 (1975).